Optimization Framework of a Ram Air Inlet Composite Morphing Flap

Carrillo Córcoles, X.; Sodja, J.; De Breuker, R.

DOI
10.7712/150123.9788.444474

Publication date
2023

Document Version
Final published version

Published in
SMART 2023

Available online at www.eccomasproceedia.org
Eccomas Proceedia SMART (2023) 317-330

ECCOMAS
Proceedia

X ECCOMAS Thematic Conference on Smart Structures and Materials
SMART 2023
D.A. Saravanos, A. Benjeddou, N. Chrysochoidis and T. Theodosiou (Eds)

OPTIMIZATION FRAMEWORK OF A RAM AIR INLET COMPOSITE MORPHING FLAP

Xavier Carrillo Córcoles*, Jurij Sodja* and Roeland De Breuker*

Department of Aerospace Structures and Materials, Delft University of Technology
Kluyverweg 1, 2629HS Delft, The Netherlands
e-mail: X.CarrilloCorcoles@tudelft.nl, J.Sodja@tudelft.nl, R.DeBreuker@tudelft.nl

Key words: Ram Air Inlet, Morphing Flap, Laminate Thickness, Multi-objective Optimization

Abstract. The ram air inlets flaps are used in some aircraft to modulate the amount of ram air cooling the Environmental Control System. The current flap design features two metallic plates connected with a hinge. The present work studies an alternative design that replaces the metallic plates with a single composite laminate with morphing capabilities. An optimization framework is proposed to define the thickness distribution of the laminate taking into account the desired operational shapes, manufacturing guidelines and maximum allowable strains. This framework combines linear and nonlinear simulations to account for the large deflections while limiting the computational cost of the optimization. The results of the optimization framework are discussed at the end of the paper and next steps are formulated.

1 INTRODUCTION

The ram air inlet flap is a system used to modulate the amount of ambient ram air, which is required to cool the main and primary heat exchanger of the Environmental Control System (ECS) on board of transport category aircraft [1]. An example of the system mounted at the lower side of the fuselage of the A380 is presented in Figure 1 [2], showing that the flap is composed of two metallic plates connected by a hinge. Furthermore, the assembly is moved by an actuator, which changes the vertical displacement of the plates, resulting in the opening and closing of the ram air inlet (RAI).

Internal Airbus studies showed that a redesign of the flap assembly could result in better performance, leading to smaller RAI systems and hence a weight reduction in future aircraft. For this reason, an alternative design is being considered. Similarly to the idea presented by Daynes and Weaver [3], it is proposed to replace the metallic plates with a single variable thickness laminate with morphing capabilities such that the RAI can operate as desired.

Therefore, this study presents the optimization framework used to design the morphing surface. The framework uses a combination of geometrically linear and nonlinear simulations to obtain the shapes of the flap and accounts for the desired flap shapes at different flight conditions, the geometry of the RAI, manufacturing guidelines and a maximum allowable strain.

Peer-review under responsibility of the organizing committee of SMART 2023.
doi: 10.7712/150123.9788.444474

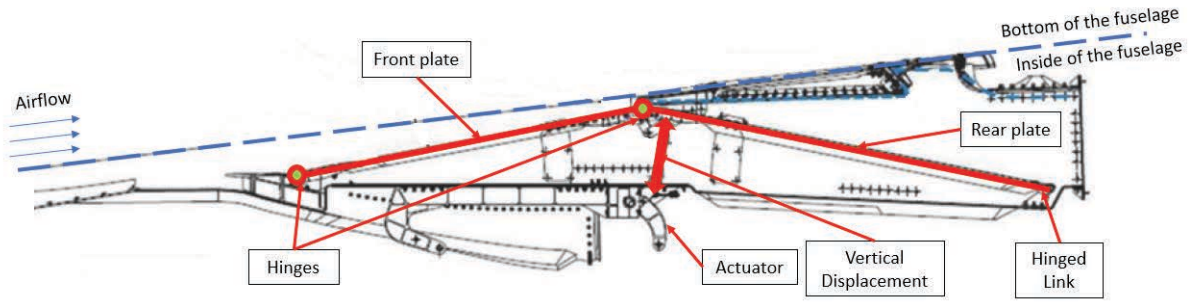

Figure 1: Cross-sectional side-view of a Airbus A380 ram air inlet. Retrieved and edited from Menga et al. [2].

2 OPTIMIZATION FRAMEWORK

The optimization framework is set up using the genetic algorithm (GA) from Matlab [4], which is connected to simulations running in Simcenter Nastran [5]. The results are recovered using pyNastran [6]. An overview of the different elements of the framework is presented in this section.

2.1 Finite element model

The finite element model (FEM) used in the simulations within the optimization is built in Simcenter 3D [7] to be solved using Simcenter Nastran [5]. The model is based on the geometry of a commercial short range aircraft RAI and consists of the composite plate and the aluminium parts that connect the plate to the RAI and the actuator. Furthermore, the plate and the aluminium supports are modelled as 2D SHELL elements and the hinges are modelled as 1D PBUSH elements. Finally, the model, which was obtained using a convergence study, is composed of a total of 28639 elements and is presented in the left-hand side figure of Figure 2.

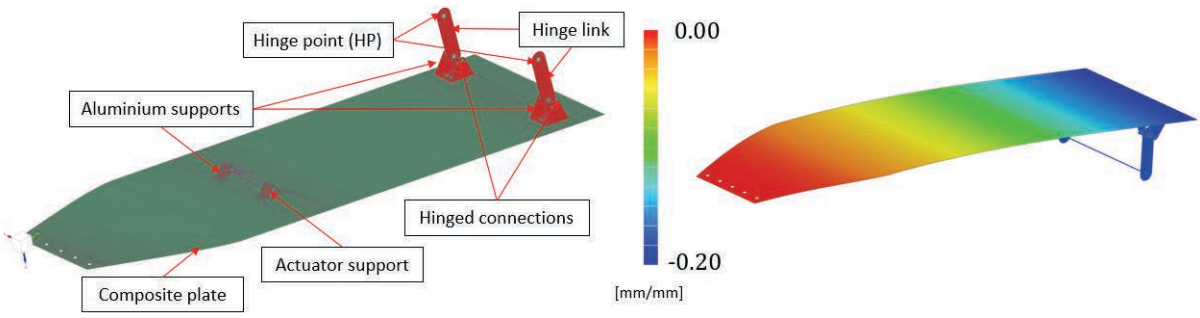

Figure 2: FEM detail. Perspective view from bottom side (left) and vertical displacement after *Initial* simulation normalised with duct length (right).

The flap is modelled as a flat plate that will later be deflected into the unloaded predeflected shape. Therefore, a first simulation using the nonlinear SOL 402 is used to enforce the boundary conditions at the hinge point (HP), which is defined by the air inlet geometry: the flap is clamped

at the root and a displacement is enforced at HP. The result of this first simulation, referred to as the *Initial* condition, can be visualized in the right-hand side figure of Figure 2.

Next, this result is used as starting point for the studied operational conditions. In these simulations, the displacement is enforced at the actuator axis and the hinge point is fixed at its position while allowed to rotate around the hinge axis. This step is conducted with the linear solver SOL 101. As further explained in Section 2.7, the linear solver is used to limit the computational cost of the optimization but will require a post-processing step to check the nonlinear results.

2.2 Flight conditions

The optimization procedure considers three operational conditions: *Open*, *Cruise* and *Closed*. On the one hand, *Open* and *Closed* correspond to taxiing and stand-still conditions, in which the RAI is completely open and closed, respectively. Given the reduced airspeed, the aerodynamic loads in these conditions are considered negligible. On the other hand, the RAI is partially closed in the *Cruise* condition. In this case, the aerodynamic loads cannot be neglected. However, a sensitivity analysis showed that the impact of the loads on the deflection is limited, so the aerodynamic loads are kept constant during deformation to simplify the problem. Therefore, in the *Cruise* condition, aerodynamic loads obtained from Airbus internal CFD studies are applied to the laminate.

2.3 Objectives

The purpose of the optimization is to obtain the thickness distribution that allows the flap to match the desired objective shapes at each of the flight conditions. Therefore, as shown in Figure 3, a different objective shape is considered for each flight condition. Notice that there is an element at the normalised horizontal position, $\overline{Y} \approx 0.7$, with which contact has to be avoided when deflecting the flap. Therefore, the *Cruise* and *Closed* objective shapes account for a certain offset distance to this internal element.

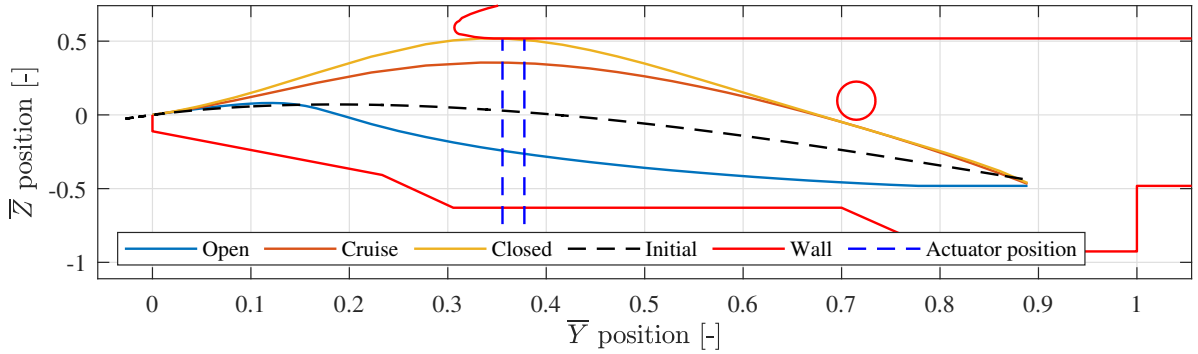

Figure 3: Comparison of objective shapes between the different flight conditions. Normalised with duct length and downstream duct height.

2.4 Constraints

The design space is constrained by the manufacturing guidelines provided by GKN, who provided input to ensure the manufacturability of the design. Furthermore, the material used is a carbon fibre PPS 5-harness weave fabric [8]. From these guidelines, it is important to (i) keep the laminate as balanced as possible, (ii) drop plies in the mid-plane instead of the outer surfaces, (iii) drop the plies far from support edges and (iv) keep a ratio between ply thickness and the distance between ply drop-offs of at least 1:20.

As a result of these guidelines, it is decided to limit the directions of the plies to $0°/90°$ and $\pm 45°$ to facilitate the laminate being balanced (i). Therefore, the stacking sequence is limited to alternating $0°/90°$ and $\pm 45°$ plies and is forced to be symmetric about the mid-plane (i). The plies are dropped at the mid-plane (ii). In addition, the laminate is discretised in the longitudinal direction ($y - \hat{j}$ direction in Figure 4) in 110 elements, E_j, of constant thickness, such that the distance between ply drop-offs is adequate (iv). These elements are represented in blue in Figure 4.

Finally, the minimum thickness of the laminate is limited to 6 plies to be able to use aerospace standard bolts [9], which show an adequate fatigue behaviour as per internal studies from GKN. In addition, based on these studies, GKN proposes a maximum allowable strain of 4000 $\mu\varepsilon$, which is also included in the optimization. However, the worst principal strains are averaged and only evaluated at the regions, $R_{j,i}$, presented in Figure 4, as it is known from previous experimental work that the most critical strains occur at the regions near the attachment holes. This way, it is possible to reduce the impact of local strain concentrations on the optimization output while still considering the critical strain regions.

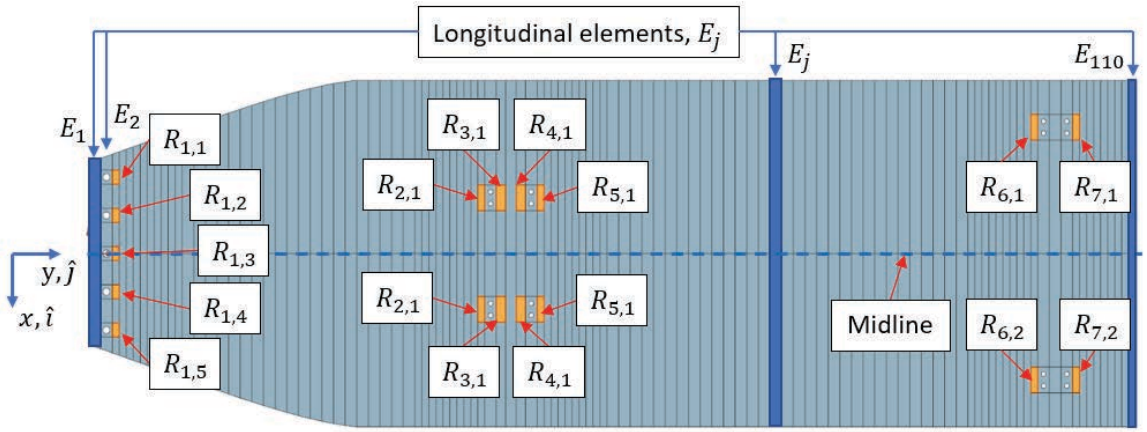

Figure 4: Detail of the longitudinal discretisation of the plate and the regions where the strains are evaluated.

2.5 Optimization problem

For the optimization problem, each design considered by the algorithm is defined by 5 regions of thickness n_i and length l_i, where n_i defines the number of plies in that region and l_i defines

the number of discrete longitudinal elements, E_j, in the region. In addition, each operative condition (*Open*, *Cruise* and *Closed*) has an extra design variable, a_i, that defines the actuator displacement. Therefore, the array of variables defining each design would be:

$$\mathbf{x} = [n_1, n_2, n_3, n_4, n_5, l_1, l_2, l_3, l_4, a_{open}, a_{cruise}, a_{closed}] \tag{1}$$

Then the final optimization problem with $g(\mathbf{x})$ as fitness function is defined as:

$$\begin{aligned} \underset{\mathbf{x}}{min} \quad & g(\mathbf{x}) \\ \text{subject to} \quad & 6 \leq n_i \text{ [plies]} \leq UB \\ & 1 \leq l_i \text{ [elements]} < 110 \\ & \textstyle\sum_{i=1}^{i=4} l_i < 110 \\ & a_{open,min} \leq a_{open} \text{ [mm]} \leq a_{open,max} \\ & a_{cruise,min} \leq a_{cruise} \text{ [mm]} \leq a_{cruise,max} \\ & a_{closed,min} \leq a_{closed} \text{ [mm]} \leq a_{closed,max} \end{aligned} \tag{2}$$

where the boundaries for the actuator displacements are defined considering the initial deflection and the objective shapes, and the upper boundary (UB) for the laminate thickness is a parameter studied in a sensitivity analysis. In addition, for practical reasons when setting up the simulations, all the variables are defined such that they can only take integer values.

Finally, as can be seen in Equation 2, the maximum material allowable is not included as a constraint. This is because, due to the architecture of Matlab optimization functions, it is not efficient to evaluate the results of the simulation to compute both the fitness function and the constraints. For this reason, the strain constraint is incorporated into the fitness function as a soft constraint. Therefore, the final fitness function is a sum of objective shapes and the maximum allowable strain constraint, which are presented in the following sections.

2.5.1 Objective shape

Three different positions of the flap are considered for the objectives, corresponding to the previously mentioned flight conditions. For each of them, the shape taken by the flap for a given laminate design is compared to the objective. At the midline of the flap, an error function, $\varepsilon(y)$, is defined as a function of the vertical deflection, z, and the objective vertical deflection, $z_{objective}$:

$$\varepsilon(y) = z(y) - z_{objective}(y) \tag{3}$$

Then, this error is included in a fitness function, f_i, with a binary constant, M, that determines in which region of the flap the function is active, and a constant, n, determining the importance of a specific region:

$$f_i(y) = M \left|\varepsilon(y)\right|^n \tag{4}$$

where $|\varepsilon(y)|$ is the absolute value of the error function, ε, at a longitudinal position, y.

Therefore, this function would allow giving more importance to the shape in specific regions, such as close to the internal element shown in Figure 3, or less importance, such as the part that is clamped at the leading edge. Finally, this function is evaluated at the nodes of the midline (N_{nodes}) and normalised with C_n to obtain a total penalty, F_i:

$$F_i = \frac{\sum_{j=1}^{j=N_{nodes}} f_i(y_j)}{C_n} \tag{5}$$

where C_n is chosen to achieve similar orders of magnitude in the penalties of the objective shapes and the penalties related to the strain constraints. Finally, this procedure is repeated for each of the conditions to obtain the *Open* penalty, F_{open}, *Cruise* penalty, F_{cruise}, and *Closed* penalty, F_{closed}.

2.5.2 Maximum allowable strain

The maximum allowable strain, introduced in Section 2.4 and evaluated in the regions from Figure 4, is included in the fitness function using a binary approach: when the average strains are above the desired threshold, a penalty is added to the objective function.

In addition, two strains are considered: the linear strains, those produced when deflecting from the *Initial* shape to the given condition (strain increment), and the nonlinear strains, from the flat flap shape to the given condition.

Finally, the penalty, S_i, for each of the conditions is computed as the ratio between the number of regions above the strain threshold and two times (linear and nonlinear) the number of regions, $R_n = 18$:

$$S_i = \frac{N_{rl} + N_{rnl}}{2R_n} \quad 0 \leq S_i \leq 1 \tag{6}$$

where N_{rl} and N_{rnl} are the number of regions above the strain allowable in the linear and nonlinear case respectively.

2.5.3 Final implementation

The final objective function, $g(\mathbf{x})$, is then a sum of the presented penalties. However, due to the penalty definition within Matlab's GA function, it is good practice to define the problem as a minimization problem with a negative minimum. Therefore, $g(\mathbf{x})$ is defined as:

$$g(\mathbf{x}) = -6 + F_{open} + F_{cruise} + F_{closed} + S_{open} + S_{cruise} + S_{closed} \tag{7}$$

where the best result would be:

$$g(\mathbf{x_{best}}) = -6 \tag{8}$$

2.6 Post-processing

As previously seen, the optimization provides a design with five regions of different thicknesses. However, a smooth transition between regions is not enforced. In addition, the ply-drop-off can also occur close to the edge of a support, which would also violate the manufacturing guidelines. Therefore, the first post-processing step is to manually modify the design to enforce the design guidelines.

Next, the optimization procedure uses linear simulations to speed up the process. However, large displacements occur between the *Initial* condition and the operational conditions, so the linear assumption has to be considered carefully.

For this reason, for the final assessment of the results, the modified output of the optimization is simulated using the nonlinear SOL 402. This time, not only the *Initial* condition is assessed but also the operational conditions (ie. *Open*, *Cruise*, *Closed*).

Finally, the results from SOL 402 are used to evaluate the fitness function as presented in Section 2.5. However, the strains require modifications. The "linear" strains are computed as the difference between the strains in the operational conditions and the *Initial* condition. Then, the nonlinear strains are those obtained directly from the respective simulation in *Open*, *Cruise* and *Closed* conditions.

2.7 Final procedure

As introduced in previous sections, the optimization procedure consists of a combination of linear and nonlinear simulations to make the procedure affordable in terms of computational costs. While the time it takes to solve the linear simulations is in the order of seconds, the nonlinear simulations take up to an hour. Therefore, since the objective is to include these simulations in an optimizer, which will run thousands of simulations, the cost of using the fully nonlinear model would be prohibitive. For this reason, linear simulations are used in the optimization while nonlinear simulations are used in the pre- and post-processing steps. The complete procedure is presented in the block diagram of Figure 5.

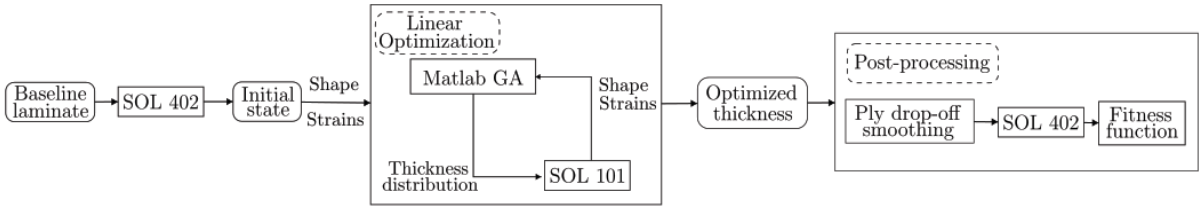

Figure 5: Block diagram of the optimization procedure.

First, a uniform thickness distribution of 8 plies is used as a reference to determine the *Initial* condition, when the laminate is assembled in the RAI but no displacement is applied to the actuator. This first step is conducted using the nonlinear solution, as explained in Section 2.1. Next, the linear optimization using the parameters presented in the previous sections is conducted around this *Initial* condition. Finally, the output of the optimization is post-processed following the steps from Section 2.6.

3 RESULTS

The results of the optimization procedure are presented in this section. First, the linear optimization is used to assess the sensitivity of the design to the maximum thickness constraint and find trends in the thickness distribution. Next, the designs obtained from the linear optimization, are evaluated again using the nonlinear solver. Finally, one of these designs is selected for further refinement.

3.1 Linear optimization

The optimization is run with different values of the maximum thickness (UB) to assess the sensitivity of the design. Table 1 presents the output for different values of UB, named UBXX where XX is the maximum number of plies, and Figure 6 shows the respective thickness distributions. In addition, a reference case with forced uniform thickness and an upper boundary of 26 plies is used to assess the maximum achievable fitness with a uniform laminate. The optimal design resulting from this reference optimization is a 14-plies laminate.

Table 1: Optimization outputs for different upper boundary values (UB).

Laminate	Output design $\mathbf{x}$									$g(\mathbf{x})$
	n_1	n_2	n_3	n_4	n_5	l_1	l_2	l_3	l_4	
UB10	6	10	10	10	8	53	30	7	19	-2.6913
UB12	12	6	7	12	12	9	38	6	51	-4.0565
UB14	13	8	6	11	14	7	25	15	2	-4.3087
UB26	21	10	6	9	22	6	19	20	9	-4.3492
Reference	14	-	-	-	-	-	-	-	-	0.0802

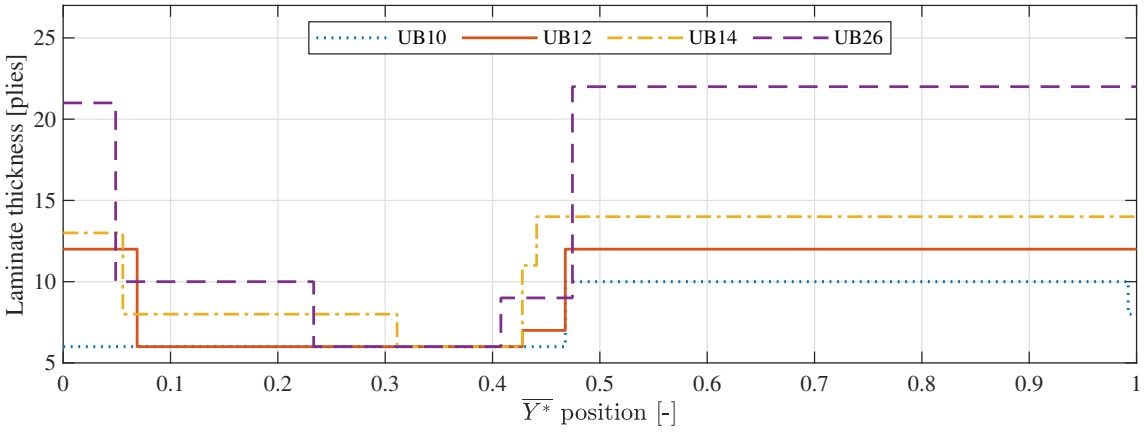

Figure 6: Comparison of laminate thickness distribution of the different outputs of the linear optimization. Longitudinal position normalised with laminate length.

Table 1 shows that increasing the UB provides an improvement in the fitness value. However, the increase of the fitness between an UB14 and UB26 is of the order of 1%. Since such an

increase in the number of plies would substantially increase the weight of the flap, the UB26 laminate will not be further considered. In addition, all the designs provide considerably better fitness values than the Reference laminate.

There is a clear trend when looking at the thickness distribution: the thickness at the clamped leading edge ($\overline{Y^*} = 0$, being $\overline{Y^*}$ the longitudinal position normalised with laminate length) and the trailing edge ($\overline{Y^*} > 0.5$) are higher than in the central region, where the actuator is attached.

3.2 Nonlinear evaluation

Next, the designs from Table 1 are post-processed and simulated again in a nonlinear simulation. Table 2 presents a summary of the fitness values and how they are distributed between the different parameters presented in Section 2.5.

Table 2: Fitness results and penalty distribution for each of the optimization output laminates after the ply drop-off smoothing post-processing step.

Laminate	F_{open}	F_{cruise}	F_{closed}	S_{open}	S_{cruise}	S_{closed}	$g(\mathbf{x})$
UB10	1.0794	0.9577	0.7155	0.0000	0.3333	0.1667	-2.7474
UB12	1.4225	0.0904	1.2657	0.0000	0.1667	0.2778	-2.7770
UB14	0.5291	0.0772	1.0486	0.0000	0.0000	0.1667	-4.1785
Reference	0.7028	0.2019	1.5489	0.3333	0.2778	0.7778	-2.1575

When looking at the shape penalties, UB12 and UB14 present low F_{cruise} penalties, which indicate good agreement with the *Cruise* objective shape. However, F_{open} for UB14 is approximately 35% of the penalty for UB12, which shows UB14 is better when matching the *Open* objective shape. Finally, F_{closed} presents a high penalty for all the laminates.

As will be discussed in Section 3.3, the *Closed* shape does not completely close the RAI, which is caused by a combination of a numerical and a design problem. The shapes used to compute the penalties are obtained as the last step of the nonlinear simulation, which fails to converge when applying higher displacements. The reason behind this convergence issue is that the laminate is not sufficiently long to close the RAI. Therefore, the loads increase abruptly when enforcing a displacement above a certain value due to the flap in-plane stiffness. Therefore, since the convergence depends on the load variation, the simulation cannot converge.

When it comes to manufacturing allowables, UB14 presents the best results, showing strains above the allowable threshold only in *Closed* condition. As can be seen in Figure 7, there is a strain concentration around the holes to which the actuator is attached ($R_{2,i}$ and $R_{5,i}$ in Figure 4). Furthermore, there is a negative strain concentration at $\overline{Y} \approx 0.1$, which coincides with the first thickness transition. Therefore, since the strain concentration is outside of the considered regions, it is not accounted for in the fitness function.

From these results, the UB14 laminate presents the best fitness value, which is approximately 30% better than the next best laminate, UB12. Therefore, UB14 is selected for further studies.

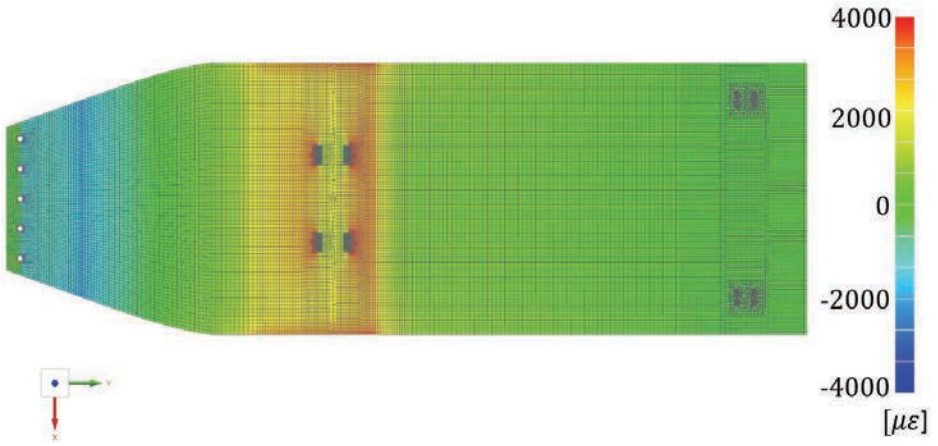

Figure 7: Worst principal strain distribution in *Closed* condition for UB14 after post-processing.

3.3 Final design

The nonlinear results from the previous section present two problems: (i) the strain concentration close to the leading edge due to the short transition from 14 plies to 8 plies and (ii) the design not being able to close the RAI completely. For this reason, two modifications to the design are proposed: (i) smoothing the thickness transition and (ii) increasing the length of the hinge link, shown in Figure 2, to facilitate closing the RAI.

Therefore, Figure 8 presents the comparison of the design obtained from the linear optimization, the design after the manual modification of the laminate thickness distribution, referred to as "refined", and the final thickness distribution, in which the transition from 14 plies to 8 plies at the leading edge of the laminate has been smoothened. As mentioned in Section 2.6, the optimization output laminate required smoothing the ply drop-offs as well as avoiding thickness changes in the proximity of a support edge, which can be observed when comparing the optimization output with the refined output.

Table 3: Comparison of fitness values and penalties before and after including the design modifications to UB14 laminate.

Laminate	F_{open}	F_{cruise}	F_{closed}	S_{open}	S_{cruise}	S_{closed}	$g(\mathbf{x})$
Refined	0.5291	0.0772	1.0486	0.0000	0.0000	0.1667	-4.1785
Final	0.7125	0.0284	0.3534	0.0000	0.0000	0.2222	-4.6835

Finally, Figure 9 to 12 present the results of the final design. As shown in Table 3, the total fitness value improves mainly due to the reduction of the shape penalty in the *Closed* condition, F_{closed}. With the hinge link modification, it is possible to close the RAI, as shown in Figure 11, so the agreement with the objective increases substantially. Nevertheless, the shape penalty in the *Open* condition, F_{open}, increases. Since the link length has been increased to be able to close the ram air inlet, the trailing edge position has changed, as shown in Figure 9. Therefore, given that the objective has not been modified, the penalty after the design modification increases.

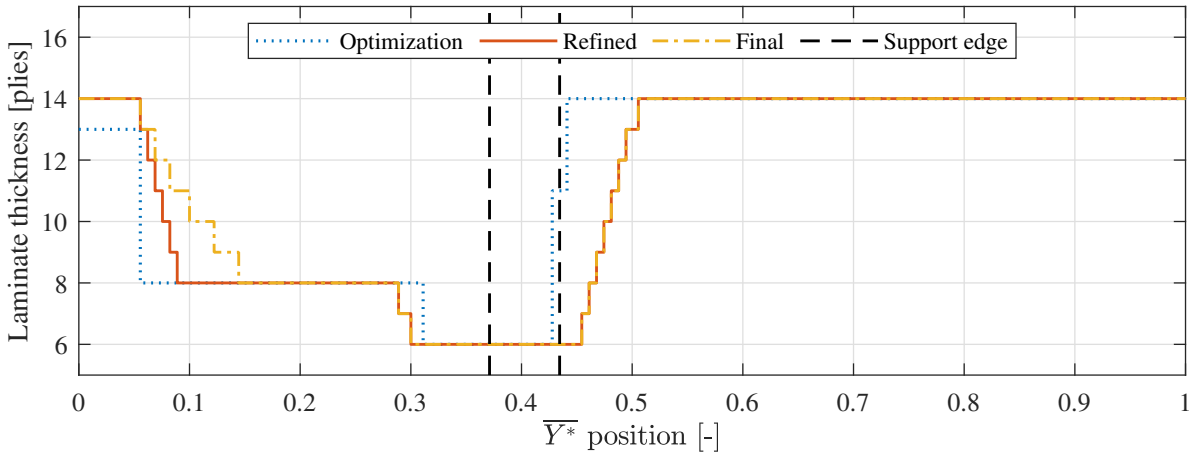

Figure 8: Comparison of laminate thickness distribution of UB14 in the different steps of the post-processing. Longitudinal position normalised with laminate length.

In addition, the shape of the trailing edge region in the open case has a reduced importance, so the increase in penalty is not as important for the final design. To conclude with the shapes, an almost negligible penalty is achieved in the *Cruise* condition, which shows good agreement in this flight condition.

To conclude, the strain penalties, S_{open}, S_{cruise} and S_{closed}, show that strains above the maximum allowable are only achieved in the *Closed* condition. As can be seen in Figure 12, the strain concentration in *Closed* condition due to the thickness change towards the leading edge is better distributed than in Figure 7. However, the strains in R_2 and R_5 are still above the allowable strain threshold. Since this is a local effect around the holes, this might be reduced with a reinforcement of the holes. In addition, notice that there has been an increase in the penalty, S_{closed}, which is due to the increment in the final displacement, and hence the loads as explained in Section 3.2, to achieve the *Closed* condition.

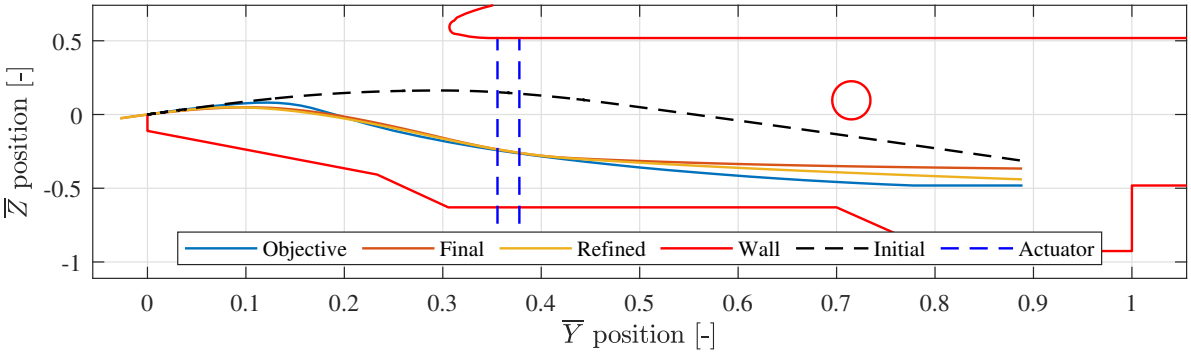

Figure 9: Comparison of *Open* shape between objective, refined UB14 and final UB14. Normalised with duct length and downstream duct height.

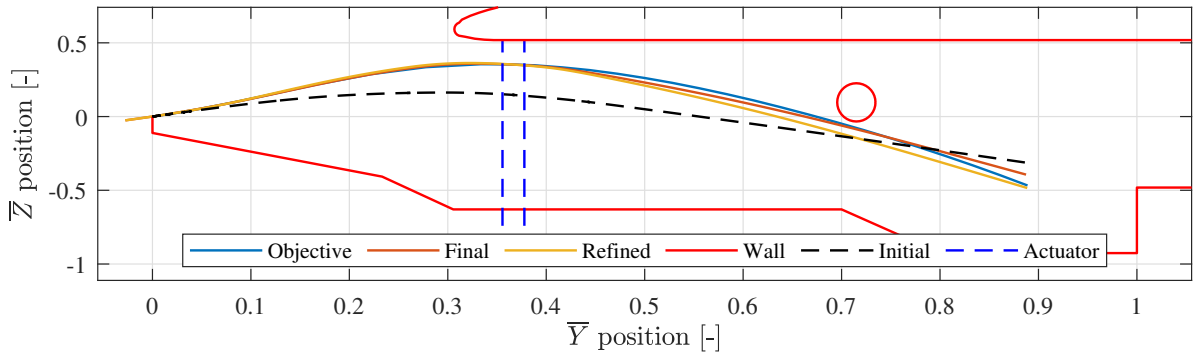

Figure 10: Comparison of *Cruise* shape between objective, refined UB14 and final UB14. Normalised with duct length and downstream duct height.

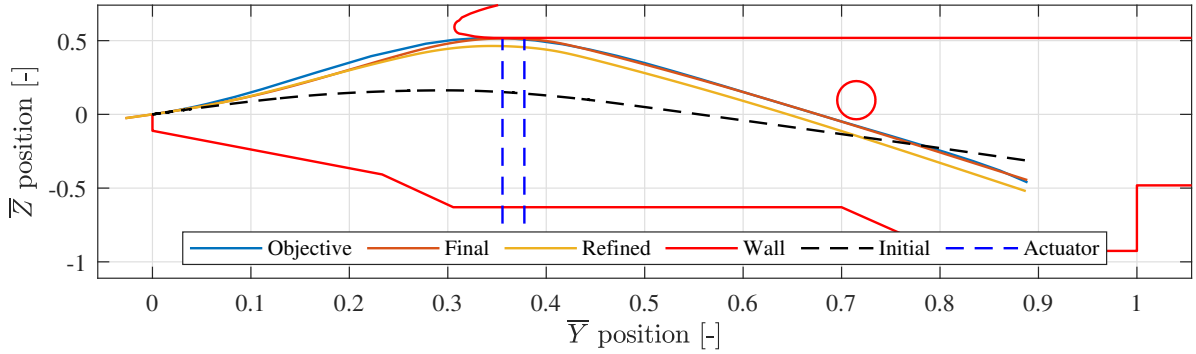

Figure 11: Comparison of *Closed* shape between objective, refined UB14 and final UB14. Normalised with duct length and downstream duct height.

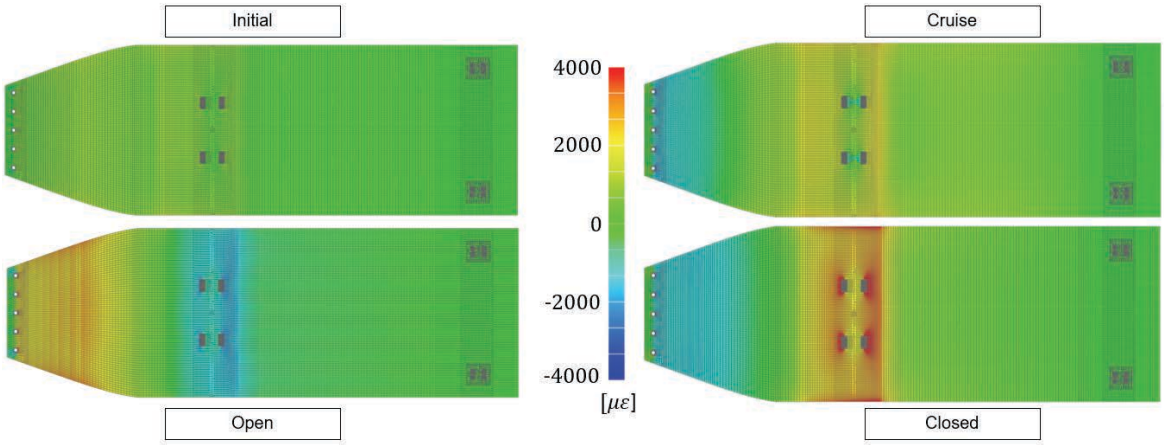

Figure 12: Worst principal strain distribution for final UB14 laminate in the different studied conditions: *Initial* (top left), *Open* (bottom left), *Cruise* (top right) and *Closed* (bottom right).

4 CONCLUSIONS

This study considers a redesign of the ram air inlet flap assembly, which allows for regulating the amount of ram air flowing into the Environmental Control System. A carbon fibre thermoplastic laminate with varying thickness is proposed to replace the current assembly, which features two metallic plates connected with a hinge.

In order to design this laminate, this study proposes the development and use of an optimization framework to obtain a thickness distribution that allows achieving the desired flap shapes while fulfilling manufacturing guidelines and constraints.

The output of this procedure is a laminate that achieves very good agreement with the desired operational shapes and only violates the maximum worst principal strain allowable locally at the region where the actuator is attached. Nevertheless, it has been seen that it is necessary to redesign the assembly, as the original dimensions did not allow closing the ram air inlet. Therefore, it is necessary to increase the length of the hinged element connected to the trailing edge of the laminate.

To conclude, this framework shows the possibility of optimizing the thickness distribution of a laminate to achieve the desired shape for different operational conditions. Therefore, this procedure has been demonstrated to be a good baseline for the design of laminates with large morphing capabilities.

ACKNOWLEDGEMENTS

This study is part of the MovAbles for Next generaTion Aircraft project (MANTA). This project has received funding from the Clean Sky 2 Joint Undertaking under the European Union's Horizon 2020 research and innovation programme under grant agreement No CS2-AIR-GAM-2014-2015-O1. Cf. Art.29.4 of [A2]. The authors also would like to thank GKN and Airbus GmbH for their input as partners in MANTA.

References

[1] "Aircraft air conditioning heat exchangers and atmospheric fouling," *Thermal Science and Engineering Progress*, vol. 7, pp. 184–202, 2018, https://doi.org/10.1016/j.tsep.2018.06.007.

[2] E. Menga, C. López, S. Hernandez, A. Baldomir, I. Romero, and M. Sánchez, "Uncertainty quantification in the dynamic response of assembled structures," in *17th International Forum on Aeroelasticity and Structural Dynamics (IFASD 2017)*, May 2017.

[3] S. Daynes and P. M. Weaver, "Stiffness tailoring using prestress in adaptive composite structures," *Composite Structures*, vol. 106, pp. 282–287, 2013, https://doi.org/10.1016/j.compstruct.2013.05.059.

[4] "Genetic Algorithm," MathWorks, 2023. [Online]. Available: https://nl.mathworks.com/discovery/genetic-algorithm.html

[5] "Simcenter Nastran Software," Siemens PLM Software, 2023. [Online]. Available: https://plm.sw.siemens.com/en-US/simcenter/mechanical-simulation/nastran/

[6] S. Doyle, "pyNastran: A Python-based interface tool for Nastran's file formats," 2020, release 1.3.3. [Online]. Available: https://github.com/SteveDoyle2/pyNastran

[7] "Simcenter simulation and test solutions," Siemens PLM Software, 2023. [Online]. Available: https://plm.sw.siemens.com/en-US/simcenter/

[8] "Toray Cetex® TC1100 - Datasheet," Toray Advanced Composites, 2021. [Online]. Available: https://www.toraytac.com/product-explorer/products/u0I7/Toray-Cetex-TC1100

[9] "ASD-STAN prEN 6122:2005 - Aerospace series: Blind bolt, 130° flush head, high strength - preferable in composite application," The European Association of Aerospace Industries - Standarization, Brussels, Belgium, 2005.